Eurasian Journal of Physics and Functional Materials

2026, 10(1), 81-96

Corrosion of zirconium alloy before and after CrN coating deposition

B.K. Rakhadilov[1], N. Muktanova[1],
E.K. Akhmetova[2,3,*], E. Turabekov[2,3]

[1]PlasmaScience LLP, Ust-Kamenogorsk 070018, Kazakhstan

[2]Institute of Materials Science and Metallurgy, Ust-Kamenogorsk 070002, Kazakhstan

[3]D. Serikbayev East Kazakhstan Technical University, Ust-Kamenogorsk 070000, Kazakhstan

E-mail: elya.akhmetova.04@gmail.com

DOI: **10.32523/ejpfm.2026100106**

Received: 05.03.2026 - after revision

In this work, the effect of various types of heat treatment, steam and air oxidation on the structure, phase composition, and corrosion properties of the zirconium alloy E110 with a CrN coating deposited by the reactive magnetron sputtering method was investigated. It was found that at a temperature of $800\,^{\circ}C$, the coating retains a dense and homogeneous structure with high adhesion, whereas at $1100\,^{\circ}C$, partial delamination and cracking of the layer are observed due to thermal stresses. X-ray diffraction analysis showed that the main phases are represented by α-Zr and CrN. After heat treatment, slight changes in diffraction peak intensity were observed, and weak reflections that may correspond to metallic chromium were detected. Oxidation experiments in an air atmosphere at $700\,^{\circ}C$ showed that the CrN coating significantly reduces mass gain and oxidation rate compared to the uncoated alloy. Steam corrosion tests at $1100\,^{\circ}C$ confirmed that the CrN coating effectively prevents oxygen diffusion, preserving the structure and integrity of the layer. According to the results of electrochemical tests in 3.5 wt.% NaCl, the corrosion current density decreased from $3.63\ \mu A/cm^2$ to $1.03\ \mu A/cm^2$, and the corrosion rate decreased from 0.0053 mm/year to 0.0000185 mm/year. The obtained data indicate that optimal heat treatment at $800\,^{\circ}C$ followed by steam oxidation ensures the formation of a durable, heat-resistant, and corrosion-resistant CrN coating that effectively protects the zirconium alloy E110 from aggressive environments.

Keywords: CrN coating; magnetron sputtering; zirconium alloys; corrosion; phase composition; mechanical properties

Introduction

Zirconium alloys are widely used for the fabrication of fuel cladding, pressure tubes, fuel channels (boxes), and fuel spacer grids in almost all water-cooled

reactors: light-water reactors such as pressurized water reactors (PWR) and boiling water reactors (BWR), as well as in the Canadian-designed heavy-water reactor, Canadian Deuterium Uranium (CANDU) [1–5]. Since its use in the first commercial nuclear power plant (Shippingport) in the 1960s, Zircaloy – an alloy of zirconium and tin — has demonstrated satisfactory performance over many decades [6, 7]. However, degradation due to water-side corrosion can limit the designed service life of nuclear fuel in the reactor. A critical phenomenon is the ingress of hydrogen into the cladding during corrosion, which can lead to its embrittlement. As energy companies strive to achieve higher fuel burnup levels, the nuclear industry has made significant efforts to understand the mechanisms of corrosion and to mitigate its effects.

Nuclear reactors represent a harsh environment for components, regardless of the reactor type. The components inside the reactor core must withstand the effects of the coolant (high-temperature water, liquid metals, gas, or molten salts), mechanical loads, vibrations, intense high-energy neutron flux, and temperature gradients. Material degradation in this environment can lead to reduced performance and, in some cases, sudden failure. Particular attention within the framework of Accident Tolerant Fuel (ATF) development is given to fuel claddings, which are especially vulnerable to rapid high-temperature oxidation accompanied by hydrogen release in a water environment.

In recent decades, considerable attention has been paid to developing effective methods for protecting zirconium alloys from high-temperature aqueous corrosion under operating conditions in the core of nuclear reactors. Among the existing approaches, surface modification methods involving the application of protective coatings play a particularly important role. Such coatings not only improve corrosion resistance but also stabilize the material's structure under thermal, radiation, and mechanical influences. The literature [8–13] describes various types of coatings applied to zirconium alloys, including FeCrAl, ZrN, Cr, and CrN. For example, FeCrAl-based coatings demonstrate high thermal stability due to the formation of a passive Al_2O_3 layer, which reduces the oxidation rate of the zirconium substrate [14–16]. ZrN and $ZrSiO_4$ coatings, in turn, exhibit good chemical inertness and can be used under conditions of increased radiation exposure [17–18]. Numerous experimental studies confirm the effectiveness of these coatings under short-term thermal heating conditions.

Among the mentioned materials, chromium nitride (CrN)-based coatings are considered among the most versatile and stable for the conditions of water-cooled reactors. This material is actively studied within the framework of the ATF (Accident Tolerant Fuel) concept – fuel resistant to accident conditions. CrN possesses a number of important characteristics: high microhardness, low friction coefficient, oxidation resistance up to $900\ ^\circ C$, and chemical stability in aqueous environments [19–22]. An important protective mechanism of CrN is the formation of a stable Cr_2O_3 oxide film on the surface, which prevents further material degradation. Due to its dense ceramic structure, CrN effectively isolates the metallic substrate from aggressive factors, preserving its integrity. A number of recent studies (for example, Bai et al.[23]) confirm that CrN combines the advantages of high hardness, good adhesion, low friction, corrosion resistance,

and thermal stability, making it a versatile coating for a wide range of applications. At the same time, metallic chromium (Cr) is characterized by higher ductility and fracture toughness under deformation, as shown in the work of Jiang et al.[24]. Therefore, Cr is often used as an interlayer in Cr/CrN systems, providing a reduction in residual stresses and improved adhesion. Such multilayer structures exhibit a better combination of mechanical and protective properties compared to monolayer coatings [25].

Such coatings can be produced by various methods. Magnetron sputtering is of particular interest. During deposition by the magnetron sputtering method, a predominantly columnar microstructure is formed, consisting of oriented grains with a pronounced (111) or (200) texture [26]. Under optimal deposition conditions, the coating exhibits high density and low defect content, which ensures improved mechanical properties and durability. Modern techniques such as pulsed and high-power impulse magnetron sputtering (HiPIMS) make it possible to obtain nanostructured CrN coatings with fine-grained and uniform structures, exhibiting excellent adhesion and enhanced resistance to wear and corrosion [27, 28].

Despite the widespread interest in CrN, most existing studies are focused on multilayer coatings. At the same time, the behavior of single-layer CrN coatings under the combined influence of thermal and corrosion factors remains insufficiently studied. A comprehensive approach to evaluating such coatings under various operating conditions is also lacking, including high-temperature oxidation in air, thermal loading under deep vacuum, exposure to saturated steam, and aggressive ionic environments [29]. In this regard, conducting systematic studies using reproducible methodologies aimed at investigating the resistance of CrN coatings to various types of degradation is a relevant and important task.

The aim of this work is to study the thermal stability and corrosion resistance of single-layer CrN coatings deposited by the magnetron sputtering method on zirconium alloy substrates. To achieve this goal, a series of tests was carried out simulating various operating conditions (oxidation in an air atmosphere at elevated temperatures, heat treatment under deep vacuum conditions, exposure to saturated steam at different temperatures, and electrochemical corrosion in a chloride-containing medium). The obtained results can be used for further optimization of protective layers of zirconium claddings operating in the reactor core, as well as for the development of new materials within the framework of the ATF concept.

Material and methods (Experimental or methodology or patients and methods

Samples made of zirconium alloy E110 were used as substrates for coating deposition. Before deposition, the substrate surface was sequentially ground using abrasive paper with varying grit sizes (from P400 to P2500). The chemical composition of the alloy is presented in Table 1.

Table 1.
Chemical composition of E110 alloy, wt.% according to GOST, TU 25278.10-82.

Zr	Be	Nb	Hf	Ni	Cr	Ti	Al	O	Pb
99,5	0,003	0,9–1,1	0,01	0,02	0,02	0,007	0,008	0,1	0,005

The coatings on zirconium alloys were formed using the PVD method. The PVD process makes it possible to deposit single-layer, multilayer, and multigradient coatings, as well as coatings with a special alloy composition and structure.

The formation of CrN coatings on zirconium alloys was carried out using the PVD method with magnetron sputtering processes at the scientific center "PlasmaScience" LLP (Ust-Kamenogorsk, Kazakhstan). Before deposition, the chamber was evacuated to 3×10^{-3} Pa, and the samples were heated to a temperature of about 300 °C and etched using an ion source in an argon atmosphere under reduced pressure. The working pressure during deposition was 0.5 Pa, and the distance from the samples to the plasma source was 150 mm. During the process, the temperature was continuously monitored using a pyrometric temperature measurement system. A metallic target made of pure chromium (99.95%) was used. CrN coating deposition was carried out in an argon atmosphere, and the process was conducted in an argon–nitrogen atmosphere with varying Ar/N_2 ratios, maintained using mass flow controllers.

The single-layer coating was obtained by magnetron sputtering using the technological parameters presented in Table 2.

Table 2.
Deposition parameters of CrN coatings by magnetron sputtering method.

Coating	Ar (sccm)	N_2 (sccm)	Power (W)	Deposition time (min)
CrN	80	40	200	120

The surface morphology and cross-sectional microstructure of the coatings were examined using a scanning electron microscope (SEM) CIQTEK SEM3200 (Hefei, Anhui, China), equipped with an energy-dispersive X-ray spectroscopy (EDS) system XFlash Detector 730M-300 (Bruker), which also made it possible to determine the elemental composition of the analyzed areas [30]. Elemental analysis was carried out using an SEM–EDS system (CIQTEK SEM3200 equipped with a Bruker XFlash Detector 730M-300). The analysis was performed at an accelerating voltage of 15–20 kV using a standardless ZAF correction procedure. Elemental distribution across the coating thickness was evaluated by line-scan analysis on polished cross-sections. Crystallographic phases were identified by X-ray diffraction (XRD) using the Bragg–Brentano geometry and by grazing incidence X-ray diffraction (GXRD) at low angles with CuKα radiation (wavelength 1.5406) using an XRD-6000 diffractometer (Shimadzu).

To evaluate the stability of the coatings, the following types of thermal and corrosion tests were carried out:

1) Heat treatment in vacuum. Annealing was carried out in a tubular vacuum furnace at temperatures of 800 and 1100 °C for 4 h. The samples were placed in the working chamber of the furnace, which was then evacuated by a fore-vacuum pump to a pressure of 1 – 2 Pa, and subsequently by a turbomolecular pump to

a level of 5×10^{-5} Pa. Heating was carried out at a rate of 20 °C per 10 min up to the target temperatures of 800 °C and 1100 °C. After the holding period, the samples were not removed from the furnace but remained under vacuum until completely cooled to room temperature to prevent oxygen exposure and possible surface oxidation [31].

2) Thermal oxidation in air atmosphere. The tests were carried out at a temperature of 700 °C in a muffle furnace model VMF4-17PX, equipped with molybdenum disilicide ($MoSi_2$) heating elements, which provide a stable and uniform temperature field. The samples were held for 5 h, with extraction intervals every hour. After each cycle, the samples were cooled in air to room temperature, and their mass was measured using CRYSTAL 100 CALCE analytical balances. The obtained data were used to determine the mass gain resulting from oxide layer formation and to analyze the oxidation kinetics of the coating at the given temperature.

3) Steam corrosion resistance tests. The samples were exposed to saturated steam at a temperature of 1100 °C in a tubular furnace Zhengzhou CY Scientific CY-CVD1200-50-200 × 200-3TH-Q (China), equipped with a programmable temperature control system. Heating to the required temperature was carried out at a rate of 10 °C/min. Before the start of the tests, a flow of high-purity argon (99.9%) was introduced into the working chamber, serving as an inert carrier gas: it ensured the removal of residual air, the supply of water vapor, stabilization of the gaseous environment during the tests, and prevention of secondary oxidation of the samples during cooling. After reaching a temperature of about 400 °C, water vapor was introduced into the chamber, generated by the SG-20 S 5008 steam generator at minimal excess pressure, ensuring stable formation of saturated steam. The duration of the isothermal holding was 2 h, after which the samples were cooled to room temperature in an argon flow. TThe change in sample mass before and after the tests was determined using an analytical balance (Gosmetr, Russia) with a resolution of 0.1 mg.

4) Electrochemical corrosion tests. The corrosion resistance of the coatings was evaluated by the potentiodynamic polarization method in a 3.5 % NaCl solution at a temperature of 25 °C using a CS300M potentiostat-galvanostat. A three-electrode cell system was used in the experiment, where a silver/silver chloride electrode served as the reference electrode, and a platinum electrode was used as the counter electrode. The working area of the sample was 1 cm^2. Before the measurements, the samples were immersed in the solution for 60 min to stabilize the open-circuit potential (OCP). Polarization curves were recorded within a range of ±0.1 V from the OCP at a scan rate of 0.5 mV/s. The analysis of parameters (corrosion potential, current density, etc.) was carried out using the Tafel method with the CS Studio6 software (version 6.3) [32].

Results and Discussion

Formed Coatings

Figure 1 shows the SEM images of the CrN coatings and the results of the EDS analysis across the depth of the CrN coatings. In all cases, the surface is characterized by a dense and uniform structure without visible pores or cracks. The layer thickness is uniform along the entire length, indicating stable deposition parameters and good process reproducibility. The coating thickness determined from SEM cross-sectional images was approximately $1.8-2.0\ \mu$m. The thickness distribution was relatively uniform along the coating cross-section, indicating good reproducibility of the magnetron deposition process. The coating thickness determined from SEM cross-sectional images was approximately $1.8-2\ \mu$m. The interfacial boundary between the coating and the substrate is clearly distinguishable, with no signs of delamination, indicating high adhesion of the coating to the substrate. The observed structure is typical for coatings obtained by the magnetron sputtering method under an optimal ratio of argon and nitrogen flow rates. The results of linear scanning confirm the presence of a clearly defined boundary between the coating and the substrate.

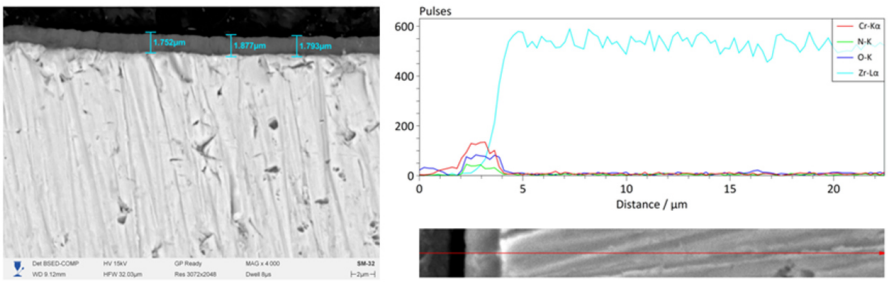

Figure 1. SEM image of CrN coatings and results of EDS analysis across the depth of CrN coatings.

The elemental composition of the coatings was determined by energy-dispersive spectroscopy (EDS) using linear scanning. Based on the obtained data, the mass (wt.%) and atomic (at.%) fractions of the identified elements were calculated (Table 3). It should be noted that EDS analysis provides only semi-quantitative information, particularly for light elements such as nitrogen and oxygen. Considering that the coating thickness ($\sim 1.8-2\ \mu$m) is comparable to the electron interaction volume in SEM–EDS analysis, the detected Zr signal may partially originate from the zirconium substrate. Therefore, the EDS results are interpreted mainly as confirmation of the presence and distribution of Cr and N within the coating rather than as an exact determination of the Cr:N stoichiometry. The linear elemental analysis (Figure 1) confirms the presence of chromium (Cr) and nitrogen (N) in the coating, with a sharp transition to zirconium (Zr) in the substrate. The oxygen (O) concentration throughout the scan is negligible, indicating the absence of oxidation of the coating in its initial state. The presence of oxygen detected in the coating composition according to the EDS analysis may be attributed to several factors, which is consistent with the data reported in the

literature for chromium nitride-based coatings obtained by the magnetron sputtering method. Firstly, during magnetron sputtering, it is difficult to completely eliminate residual partial pressures of oxygen, even at a high degree of chamber vacuum. Due to the high chemical activity of chromium, partial oxidation of the material may occur both during deposition and at the cooling stage. Secondly, after the completion of deposition and removal of the samples from the vacuum chamber, the surface comes into contact with atmospheric air. This may lead to the formation of a thin surface oxide layer, which is detected in the EDS spectrum as the presence of oxygen.

Table 3.
Elemental composition of CrN coatings.

Elements	Cr	Zr	N	O	Sum
Norm. atomic concentration, at.%	4.72	56.48	14.25	24.56	100
Norm. mass concentration, mass.%	4.09	86.01	3.33	6.56	100

Heat treatment in vacuum

The heat treatment of the samples was carried out at temperatures of 800 and 1100 °C in a vacuum tubular furnace for 4 h. Four samples were used for the analysis: two without coating (the original zirconium alloy E110) and two with a CrN coating applied. Figures 2–3 show the cross-sectional microstructures and the results of linear elemental analysis after annealing at the specified temperature conditions.

Figure 2 presents the results of studying the effect of heat treatment at 800 °C on the structure of the zirconium alloy E110 and the alloy with the CrN coating. In the cross-section of the uncoated sample after heat treatment at 800 °C (Figure 2 a,b), the linear elemental analysis shows a stable zirconium (Zr) content throughout the entire cross-sectional thickness. The oxygen (O) concentration remains at a minimal level, indicating the absence of pronounced surface oxidation. The obtained data indicate the preservation of the original structure of the E110 alloy and confirm the stability of the material at this processing temperature. In the sample with the CrN coating (Figure 2 c,d), a surface layer with a clearly defined interface between the coating and the substrate is formed. However, the SEM image shows local areas of delamination and partial loss of coating continuity, which is likely associated with thermal stresses arising from the difference in the coefficients of thermal expansion between CrN and the zirconium substrate. In certain areas, disruption of the coating–substrate contact accompanied by micropores is observed. Similar defects were reported by Jiang et al. [33], where cracks in CrN coatings on Zr-4 were observed at 400 °C, also caused by thermomechanical incompatibility. Elemental analysis confirms the presence of chromium and nitrogen in the surface layer of the coating, with a sharp decrease at the delamination boundary, indicating weak interlayer diffusion interaction. The substrate composition is predominantly represented by zirconium, with no detectable oxygen content, indicating the absence of oxidation and corresponding to the α-phase of the E110 alloy. The obtained data are consistent with the results

of Meng et al. [33], where at a temperature of 860 °C, the CrN coating retained its structure; however, initial signs of degradation similar to those observed in the present study were noted.

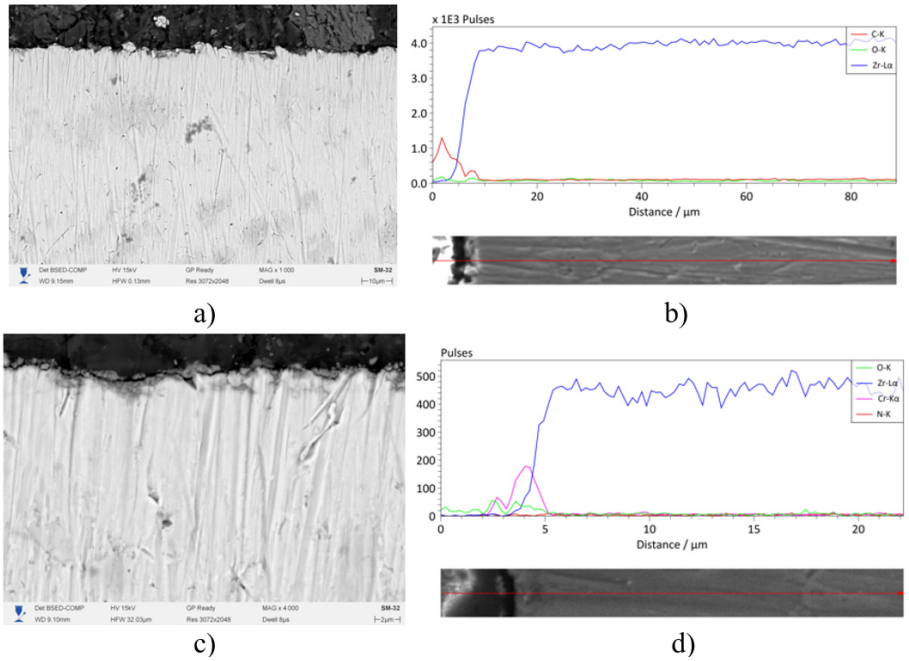

Figure 2. Effect of heat treatment at 800 °C on the structure and composition of the zirconium alloy E110 and CrN coating: (a, b) - E110 alloy; (c, d) - E110 alloy with CrN coating (SEM images and line analysis).

An increase in temperature to 1100 °C leads to more pronounced changes both in the structure of the E110 alloy and in the condition of the CrN coating (Figure 3). In the uncoated sample (Figure 3 a,b), significant grain growth and partial recrystallization of the structure are observed. The characteristic lamellar α-structure of the E110 alloy becomes less pronounced, indicating the occurrence of a reverse $\beta \rightarrow \alpha$ phase transformation during cooling after heating. Elemental analysis shows a stable zirconium content throughout the thickness and a noticeable increase in oxygen concentration in the near-surface zone, indicating intensive surface oxidation and the formation of a thickened oxide film. In the case of the alloy with the CrN coating (Figure 3 c,d), a coating layer remains on the surface; however, its structure becomes non-uniform. The SEM image reveals areas of cracking and partial delamination of the coating from the substrate. These defects are associated with the increase in thermal stresses caused by the difference in the coefficients of thermal expansion between CrN and the zirconium substrate. Linear elemental analysis confirms the presence of zones with reduced nitrogen content and increased oxygen concentration, indicating partial oxidation of the coating and the formation of mixed oxide–nitride phases. At the same time, no noticeable diffusion of chromium into the substrate is observed.

The conducted study showed that increasing the heat treatment temperature from 800 to 1100 °C leads to significant structural changes in the zirconium alloy E110 and degradation of the CrN coating. For a more detailed analysis of the occurring phase transformations and to assess the stability of compounds in the CrN–E110 system after heat treatment, X-ray diffraction (XRD) analysis was

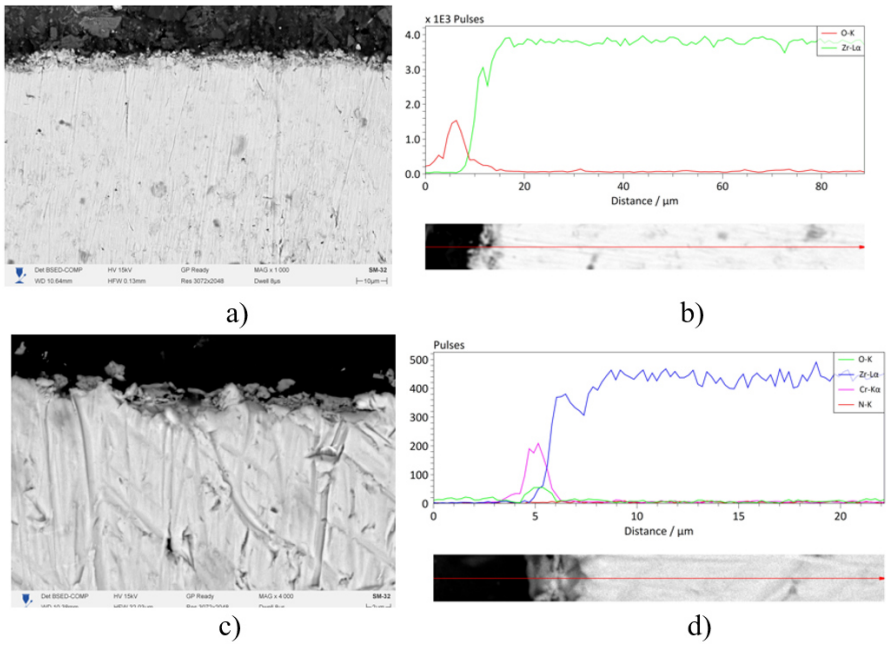

Figure 3. Effect of heat treatment at 1100 °C on the structure and composition of the zirconium alloy E110 and the CrN coating: (a, b) - E110 alloy; (c, d) - E110 alloy with CrN coating (SEM images and line analysis).

carried out.

Figure 4 shows the X-ray diffraction pattern of the zirconium alloy E110 with a CrN coating after heat treatment at different temperatures (800 °C and 1100 °C).

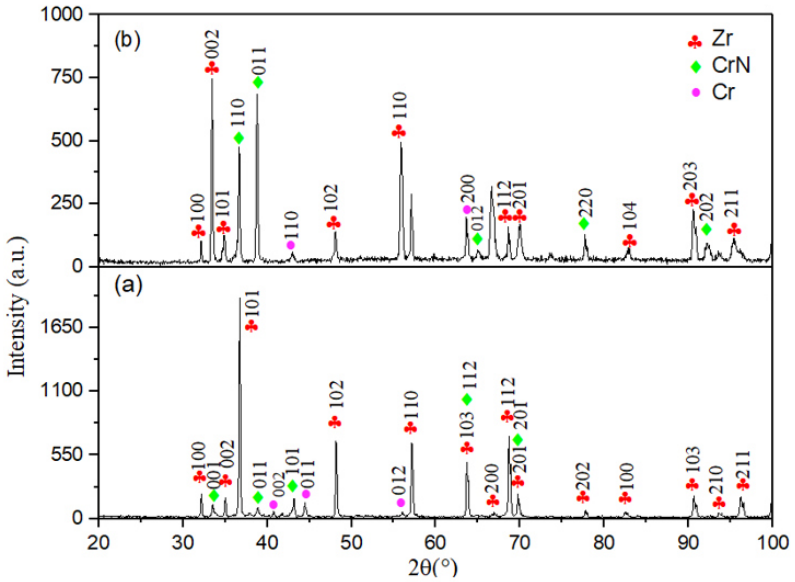

Figure 4. X-ray diffraction analysis of the zirconium alloy E110 with CrN coating before (a) and after heat treatment at 800 °C (b) and 1100 °C (c).

In the initial state (Figure 4 a), the diffraction pattern contains well-defined peaks characteristic of the CrN coating and the zirconium alloy substrate. The high intensity of the reflections indicates an ordered crystalline structure and the absence of foreign phases.

After heat treatment at 800 °C (Figure 4 c), the main peaks are retained; however, their intensity slightly decreases. This is associated with partial relaxation of internal stresses and minor changes in the microstructure of the coating. At

the same time, the CrN structure remains stable, confirming the thermal stability of the coating at this temperature.

After heat treatment at 1100 °C (Figure 4 b), changes in the relative intensity of several diffraction peaks are observed, which may indicate structural rearrangement and relaxation of internal stresses in the coating. The diffraction patterns show that the main phases of the system are α-Zr from the substrate and CrN from the coating. In addition to the dominant CrN reflections, weak peaks that may correspond to metallic chromium are also detected, which may be associated with partial modification of the nitride phase during high-temperature exposure.

Thus, the results of the X-ray diffraction analysis show that the CrN coating remains stable at temperatures up to 1100 °C, while the high temperature contributes to improved crystallinity and structural ordering of the material.

Oxidation Experiment: 700 °C/1, 2, 3, 4, and 5 h/air

Figure 5 shows the oxidation kinetics of the zirconium alloy E110 in the initial state (red line) and with a CrN coating (black line) at a temperature of 700 °C. Oxidation was carried out in air atmosphere for five hours, with intermediate cooling and weighing after each hour of exposure.

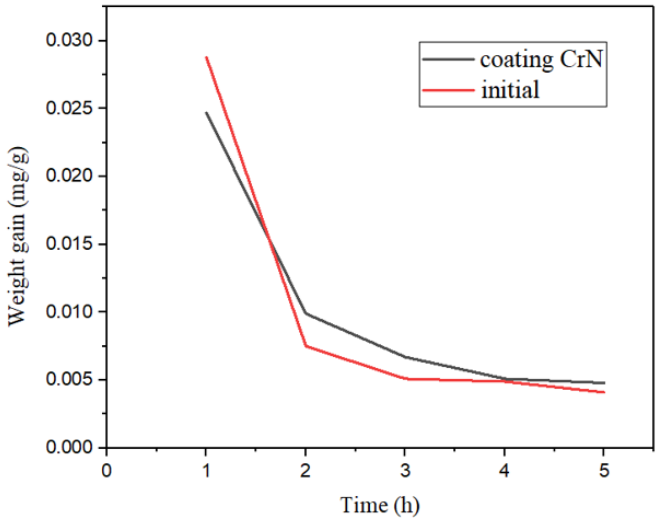

Figure 5. Mass gain of the zirconium alloy without coating and with CrN coating at 700 °C.

The unmodified zirconium alloy exhibited a more intense mass gain at the initial stages of the test, indicating a rapid oxidation process. After the first two cycles, a noticeable decrease in the mass gain rate was observed; however, the total accumulation of the oxide film remained higher than that of the CrN coating.

In the case of the sample coated with a CrN layer, the mass gain at all stages was significantly lower. This indicates that the applied coating effectively hinders oxygen diffusion and slows down the oxidation processes at 700 °C. After the completion of the fifth cycle, the mass gain of the coated sample remained significantly lower than that of the uncoated alloy, confirming the protective effect of the CrN coating (Table 4). Thus, the CrN coating provides reliable protection

of the zirconium alloy surface and enhances its thermo-oxidation resistance at high temperatures.

Table 4.
Mass gain of E110 alloy with and without CrN coating during oxidation at 700.

Time (h)	Uncoated E110 (mg/cm^2)	CrN coating (mg/cm^2)
1	10.98	12.80
2	4.40	3.33
3	2.98	2.27
4	2.27	2.18
5	2.13	1.82

To evaluate the structural changes occurring under thermal exposure in an oxidative atmosphere, SEM studies and elemental analysis of the cross-sections of E110 zirconium alloy samples — both without coating and with the applied CrN coating — were carried out after exposure at 700 °C for 5 h (Figure 6). The images (Figure 6 a,c) show the CrN coating. It is evident that the coating retains a dense, uniform structure with a clearly defined interface between the coating and the substrate. EDS maps of the Cr, N, Zr, and O elements show a uniform distribution of the main components across the coating thickness. The presence of oxygen in the near-surface zone indicates the formation of a thin oxide layer resulting from the interaction of the coating with the oxidative atmosphere under cyclic thermal exposure. The observed crack in the cross-section is not systematic and is likely caused by local thermomechanical stresses. Figures 6b and 6d present the results for the E110 zirconium alloy sample without coating after similar oxidation conditions. The BSE image shows the presence of a distinct oxide layer on the substrate surface, with a thickness of several micrometers. EDS analysis shows a significant increase in oxygen content in the surface region and a gradual decrease in Zr concentration with depth, indicating intensive oxidation of the zirconium base. Unlike the CrN coating, the oxidized layer on the E110 alloy is characterized by inhomogeneity and the presence of porous regions, which reduces its protective properties.

A comparison of coated and uncoated samples shows that the use of a CrN coating significantly enhances the thermo-oxidation resistance of the system. The coating prevents intensive oxygen diffusion and the formation of oxide phases in the substrate, ensuring the structural integrity even after multiple heating–cooling cycles at 700 °C.

Steam corrosion resistance

Figure 7 shows the cross-sectional microstructures and EDS line analysis results of the zirconium alloy with a CrN coating after steam corrosion resistance tests at 1100 °C.

The thickness of the oxide layer formed on the uncoated zirconium alloy after steam exposure at 1100 °C was approximately 14 – 15 μm, as measured from SEM cross-sectional images. The oxide scale is characterized by a heterogeneous structure and the presence of microcracks, indicating intensive oxidation and the

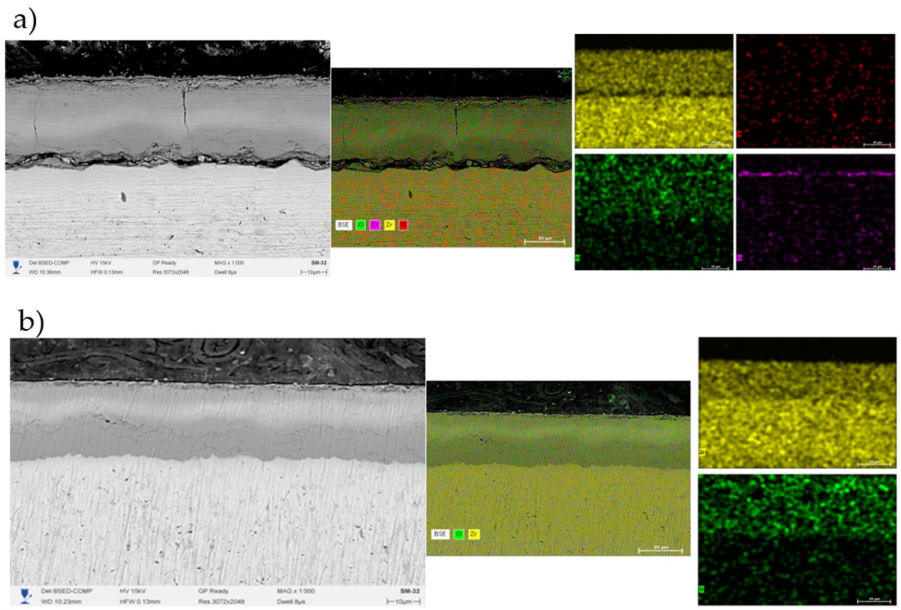

Figure 6. SEM images and EDS analysis results of CrN coatings and E110 zirconium alloy after cyclic oxidation at 700 °C : (a) - CrN coating on E110 alloy; (b) - E110 zirconium alloy without coating.

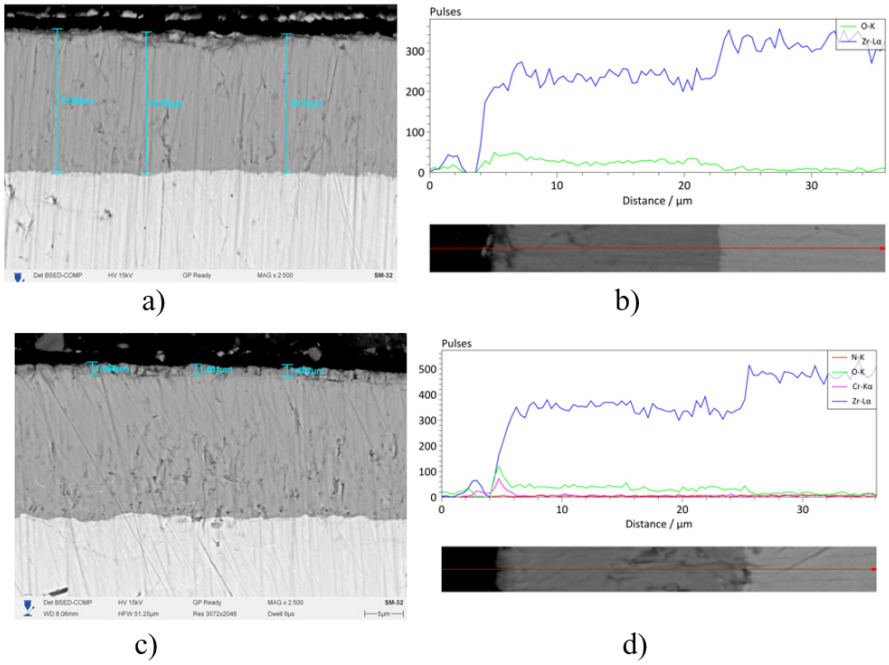

Figure 7. Cross-sections and EDS line analysis results of the zirconium alloy without coating (a, b) and with CrN coating (c, d) after steam corrosion resistance tests at 1100 °C.

development of thermal stresses under exposure to saturated steam. According to the results of the EDS line analysis, the concentration of oxygen (O-K) sharply increases in the surface zone and gradually decreases toward the metallic matrix. At the same time, the distribution of zirconium (Zr-Lα) indicates a region of deep substrate oxidation, confirming the low corrosion resistance of the alloy without a protective coating under these conditions.

In contrast, the oxide layer formed on the CrN-coated sample is significantly thinner and more uniform compared to the uncoated alloy. No pronounced cracking or delamination of the coating layer was observed, indicating good

structural stability of the coating during high-temperature steam exposure. The coating thickness averages $1.8-2.0\ \mu$m, and the interface between the coating and the substrate remains clearly defined. This value is close to the initial coating thickness, indicating that no significant degradation or loss of coating material occurred during the steam corrosion test. The EDS line analysis confirms the presence of a stable CrN layer with a uniform distribution of chromium (Cr-Kα) and nitrogen (N-Kα). The oxygen (O-K) concentration increases only in the surface region, indicating the formation of a thin oxide layer without significant oxygen diffusion into the substrate.

Thus, the comparative analysis confirms that the application of a CrN coating significantly improves the zirconium alloy's resistance to steam corrosion at 1100 °C. The coating acts as an effective barrier that limits oxygen diffusion and suppresses the formation of a thick oxide layer on the zirconium substrate.

Electrochemical corrosion

The corrosion resistance of the E110 zirconium alloy and the alloy with a CrN coating was evaluated using the potentiodynamic polarization method with an open surface area of 1 cm^2 in a 3.5 wt.% NaCl solution at room temperature (25 °C). Three tests were carried out for each sample to obtain reproducible data. The potentiodynamic polarization curves are shown in Figure 8, and the calculated electrochemical parameters are presented in Table 5.

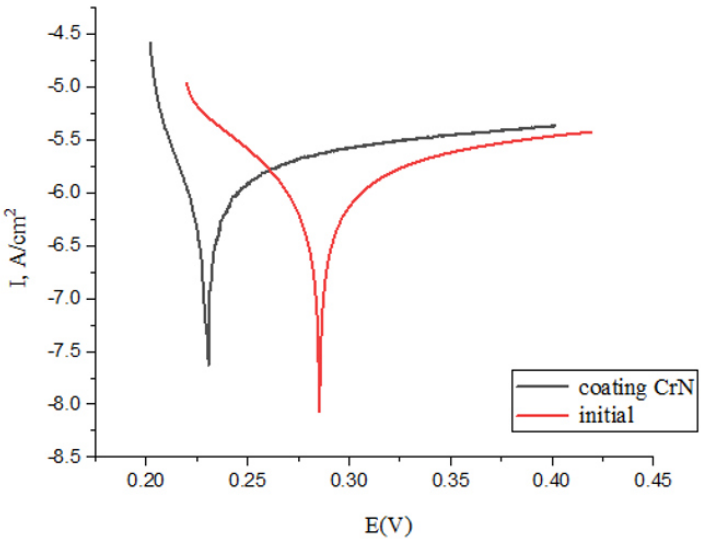

Figure 8. Potentiodynamic polarization curves of the E110 zirconium alloy and CrN coatings.

Table 5.
Corrosion test parameters of the initial and CrN-coated zirconium alloy.

Parameters	Initial	Coating CrN
E_{corr} (mV)	22.805	22.832
I_{corr} (μA/cm^2)	3.63	1.03
β_c (mV)	6.506	6.5
β_a (mV)	0.785	0.64
r_{corr} (mm/year)	0.0053041	0.0000185

To determine the average values of the electrochemical characteristics, extrapolation of the Tafel regions of the anodic and cathodic branches of the polarization curves was performed. The intersection point of these branches was used to determine the corrosion current density (I_{corr}) and the corrosion potential (E_{corr}). Detailed analysis results are presented in Table 5, where β_a and β_c denote the slopes of the anodic and cathodic branches, respectively.

According to the data in Table 5, the application of a CrN coating significantly reduces the corrosion current density and corrosion rate compared to the original alloy. For the original sample, the I_{corr} value was $3.63\ \mu\text{A/cm}^2$, whereas for the sample with the CrN coating it was $1.03\ \mu\text{A/cm}^2$. Similarly, the corrosion rate (r_{corr}) decreased from 0.0053 mm/year to 0.0000185 mm/year. Such a decrease in current density and corrosion rate indicates a significant improvement in the material's resistance to electrochemical dissolution in a chloride environment.

In addition, a slight shift of the corrosion potential (E_{corr}) toward more positive values (from 22.805 to 22.832 mV) is observed, confirming the improvement of the surface's passive properties. The decrease in the slopes of the anodic (β_a) and cathodic (β_c) branches indicates stabilization of the passive film and a reduction in the rates of the anodic and cathodic reactions.

The improved corrosion resistance of the E110 alloy with the CrN coating is attributed to the formation of a dense, low-porosity nitride layer that effectively isolates the substrate from the influence of aggressive Cl^- ions. At the same time, the barrier nature of the coating prevents the diffusion of oxygen and hydrogen, ensuring potential stability and a reduction in the overall corrosion rate.

Thus, the results of the potentiodynamic tests confirm that the application of a CrN coating significantly improves the corrosion characteristics of the E110 zirconium alloy. The coating forms a stable passive barrier that reduces the corrosion current density by more than two orders of magnitude, indicating its high protective efficiency in chloride-containing environments.

Conclusions

In this study, a comprehensive evaluation of the thermal and corrosion resistance of single-layer CrN coatings deposited by magnetron sputtering on E110 zirconium alloy substrates was carried out. Main conclusions:

1. Morphology and composition of the coating. The CrN coating is characterized by a dense, uniform structure without pores or cracks. SEM images and EDS analysis confirm a stable distribution of chromium and nitrogen throughout the layer thickness and a clear interface between the coating and the substrate, indicating high adhesion and deposition quality.

2. Thermal stability. It was found that during heat treatment at $800\ ^\circ\text{C}$, the E110 alloy structure retains the stable α-phase of zirconium, and the CrN coating remains dense and uniform. At $1100\ ^\circ\text{C}$, grain coarsening, partial recrystallization of the substrate, and the appearance of coating delamination areas occur due to thermal stresses. X-ray diffraction analysis showed that the main phases are represented by α-Zr and CrN. With increasing temperature

up to 1100 °C, changes in the relative intensity of CrN peaks are observed. In addition, weak reflections that may correspond to metallic chromium appear in the diffraction pattern, which may indicate partial modification of the nitride phase during high-temperature exposure.

3. Oxidation in air atmosphere. The CrN coating effectively slows down the formation of the oxide layer compared to the uncoated sample. At 700 °C for 5 h, a significant reduction in mass gain is observed, indicating slowed oxidation kinetics and the protective function of the coating.

4. Steam corrosion. Steam oxidation leads to the formation of a zirconium oxide layer (ZrO_2) on the surface, as observed in the SEM cross-sectional images (Figure 7). The oxide layer formed on the uncoated alloy reaches a thickness of approximately 14 – 15 μm and exhibits a heterogeneous structure with visible microcracks. In contrast, the CrN-coated sample shows a significantly thinner and more uniform oxide scale without pronounced cracking or delamination. The combined action of the CrN coating and the oxide layer provides a two-level barrier protection against oxygen and chloride diffusion, enhancing the thermal stability and chemical inertness of the surface.

5. Electrochemical corrosion. In a 3.5 wt.% NaCl solution, the application of a CrN coating reduces the corrosion current density by more than two orders of magnitude and significantly decreases the corrosion rate. The coating stabilizes the potential and reduces the activity of anodic and cathodic processes, providing effective protection against electrochemical degradation.

Thus, optimal heat treatment at 800 °C followed by steam oxidation ensures the formation of a durable, thermally stable, and corrosion-resistant CrN/ZrO_2 coating that effectively protects the E110 zirconium alloy from the effects of aggressive environments.

References

[1] A.I. Miller et al., Nuclear Engineering Handbook. Boca Raton, CRC Press (2016).
[2] Y. Han, X. Zhong, Nuclear Power Reactor Designs. Academic Press (2024) 351–363. [*CrossRef*]
[3] M. Tucker, Thesis (2023).[*Web Link*]
[4] R.L. Tapping, Nuclear Corrosion Science and Engineering. Woodhead Publishing Series in Energy, Woodhead Publishing (2012) 581–633. [*CrossRef*]
[5] E. De Sanctis, S. Monti, M. Ripani, Energy from Nuclear Fission: An Introduction. Springer International Publishing (2016) 147–187.[*Web Link*]
[6] Z. Karoutas et al., Progress in Nuclear Energy **102** (2018) 68–78. [*CrossRef*]
[7] K.D. Kok, Nuclear Engineering Handbook. Boca Raton, CRC Press (2016).
[8] Y. Su et al., Tribology **45** (2025) 1521–1533. [*Web Link*]
[9] L. Chen, Y.X. Xu, L.J. Zhang, Surface and Coatings Technology **285** (2016) 146–152. [*CrossRef*]
[10] D.V. Sidelev et al., Surface and Coatings Technology **433** (2022) 128131. [*CrossRef*]

[11] T. Kuznetsova et al., Applied Surface Science **522** (2020) 146508. [*CrossRef*]
[12] J.W. Du, H.D. Zhang, L. Chen, Y. Kong, Surface and Coatings Technology **493** (2024) 131276. [*CrossRef*]
[13] X. Han, Y. Wang, S. Peng, H. Zhang, Corrosion Science **149** (2019) 45–53. [*CrossRef*]
[14] T. Dabney et al., Nuclear Materials and Energy **21** (2019) 100715. [*CrossRef*]
[15] X. Yang et al., Surface and Coatings Technology **473** (2023) 129992. [*CrossRef*]
[16] R. Zhou et al., Materials Characterization **204** (2023) 113221. [*CrossRef*]
[17] O.G. Kryukova, T.A. Krylova, Inorganic Materials **59** (2023) 417–422. [*CrossRef*]
[18] L. Liu, W. Zheng, Z. Ma, Y. Liu, Journal of Advanced Ceramics **7** (2018) 336–342. [*CrossRef*]
[19] Y. Li et al., Tungsten **7** (2025) 50–70. [*CrossRef*]
[20] J. Lin et al., Surface and Coatings Technology **204** (2010) 2230–2239. [*CrossRef*]
[21] C.W. Luo et al., Vacuum **203** (2022) 111253. [*CrossRef*]
[22] J. Lin et al., Thin Solid Films **519** (2011) 2402–2408. [*CrossRef*]
[23] H. Bai et al., Materials **16** (2023) 6303. [*CrossRef*]
[24] J. Jiang et al., Surface and Coatings Technology **409** (2021) 126812. [*CrossRef*]
[25] F. Jasempoor et al., International Journal of Applied Ceramic Technology **19** (2022) 2222–2235. [*CrossRef*]
[26] P.H. Mayrhofer, G. Tischler, C. Mitterer, Surface and Coatings Technology **142–144** (2001) 78–84. [*CrossRef*]
[27] A. Anders et al., Journal of Applied Physics **102** (2007) 113303. [*CrossRef*]
[28] J. Paulitsch et al., Thin Solid Films **518** (2010) 5558–5564. [*CrossRef*]
[29] T. Tulenbergenov et al., Nuclear Materials and Energy **13** (2017) 63–67. [*CrossRef*]
[30] D. Buitkenov et al., Key Engineering Materials **839** (2020) 137–143 [*CrossRef*]
[31] B.K. Rakhadilov et al., Applied Physics A **128** (2022) 145. [*CrossRef*]
[32] D. Buitkenov et al., Materials **17** (2024) 5253. [*CrossRef*]
[33] C. Meng et al., Journal of Nuclear Materials **515** (2019) 354–369. [*CrossRef*]